Title
Assessing Historical Variability of South Asian Monsoon Lows and Depressions With an Optimized Tracking Algorithm

Journal
Journal of Geophysical Research: Atmospheres, 125(15)

ISSN
2169-897X

Authors
Vishnu, S
Boos, WR
Ullrich, PA
et al.

Publication Date
2020-08-16

DOI
10.1029/2020jd032977

Peer reviewed

JGR Atmospheres

RESEARCH ARTICLE
10.1029/2020JD032977

Assessing Historical Variability of South Asian Monsoon Lows and Depressions With an Optimized Tracking Algorithm

S. Vishnu[1], W. R. Boos[1,2], P. A. Ullrich[3], and T. A. O'Brien[2,4]

[1]Department of Earth and Planetary Science, University of California, Berkeley, CA, USA, [2]Climate and Ecosystem Sciences Division, Lawrence Berkeley National Laboratory, Berkeley, CA, USA, [3]Department of Land, Air, and Water Resources, University of California, Davis, CA, USA, [4]Earth and Atmospheric Sciences Department, Indiana University, Bloomington, Bloomington, IN, USA

Key Points:
- The stream function of the horizontal wind is shown to be highly skillful for identifying monsoon low-pressure systems (LPS)
- Uncertainty analyses show that previously reported trends in Indian monsoon depressions may be artifacts of changes in the observing network
- More LPS form in La Niña and wet monsoon years, but other interannual climate modes do not modulate LPS consistently across five reanalyses

Supporting Information:
- Supporting Information S1

Correspondence to:
S. Vishnu,
vishnuedv@gmail.com

Citation:
Vishnu, S., Boos, W. R., Ullrich, P. A., & O'Brien, T. A. (2020). Assessing historical variability of South Asian monsoon lows and depressions with an optimized tracking algorithm. *Journal of Geophysical Research: Atmospheres*, *125*, e2020JD032977. https://doi.org/10.1029/2020JD032977

Received 22 APR 2020
Accepted 17 JUN 2020
Accepted article online 22 JUN 2020

Abstract Cyclonic low-pressure systems (LPS) produce abundant rainfall in South Asia, where they are traditionally categorized as monsoon lows, monsoon depressions, and more intense cyclonic storms. The India Meteorological Department (IMD) has tracked monsoon depressions for over a century, finding a large decline in their number in recent decades, but their methods have changed over time and do not include monsoon lows. This study presents a fast, objective algorithm for identifying monsoon LPS and uses it to assess interannual variability and trends in reanalyses. Variables and thresholds used in the algorithm are selected to best match a subjectively analyzed LPS data set while minimizing disagreement between four reanalyses in a training period. The stream function of 850 hPa horizontal wind is found to be optimal in this sense; it is less noisy than vorticity and represents the complete nondivergent wind, even when flow is not geostrophic. Using this algorithm, LPS statistics are computed for five reanalyses, and none show a detectable trend in monsoon depression counts since 1979. Both the Japanese 55-year Reanalysis (JRA-55) and the IMD data set show a step-like reduction in depression counts when they began using geostationary satellite data, in 1979 and 1982, respectively; the 1958–2018 linear trend in JRA-55, however, is smaller than in the IMD data set, and its error bar includes 0. There are more LPS in seasons with above-average monsoon rainfall and in La Niña years, but few other large-scale modes of interannual variability are found to modulate LPS counts, lifetimes, or track length consistently across reanalyses.

1. Introduction

Cyclonic low-pressure systems (LPS) are the dominant synoptic-scale phenomena that bring rain to India and surrounding regions during the boreal summer monsoon season. With outer diameters near 2,000 km, these monsoon LPS typically form over the northern Bay of Bengal then propagate to the northwest over India during the subsequent several days (Godbole, 1977; Mooley, 1973; Sikka, 1978). Although these storms have weak surface winds of order 10 m s^{-1}, they produce abundant rainfall, with precipitation rates peaking at 3–5 cm day^{-1} in composite means and some storms producing 10–50 cm of rain along their tracks (Boos et al., 2015; Hunt et al., 2016; Sanders, 1984; Sikka, 2006). Monsoon LPS make a large contribution to the total summer monsoon rainfall of continental South Asia (Yoon & Chen, 2005) and have produced catastrophic floods there (Houze Jr et al., 2011).

Given the importance of monsoon LPS, there is great interest in studying the variability of these storms. The India Meteorological Department (IMD) has kept records on LPS since the late nineteenth century (India Meteorological Department, 2011). They traditionally categorized these storms by intensity, with the weakest systems called monsoon lows (surface wind speeds less than 8.5 m s^{-1} and mean sea level pressure (MSLP) at least 2 hPa lower than surrounding regions), stronger systems called monsoon depressions (wind speeds 8.5–13.5 m s^{-1} and MSLP anomalies 4–8 hPa), and even stronger vortices called deep depressions and cyclonic storms. The use of surface wind speed or surface pressure as a metric for categorization has varied over time (India Meteorological Department, 2011). The historical IMD data set includes only depressions and stronger storms, but Mooley and Shukla (1987) and Sikka (2006) produced a separate data set of both lows and depressions by manually identifying LPS from hand-analyzed daily weather charts of the IMD. These data sets have been used in numerous studies of variations in the number of monsoon LPS. For

example, the number of LPS forming each summer has been shown to be modulated by the El Niño–Southern Oscillation (ENSO) (Hunt et al., 2016), the Pacific Decadal Oscillation (PDO) (Vishnu et al., 2018), and the Indian Ocean Dipole (IOD) (Krishnan et al., 2011), all of which are also associated with interannual variations in the strength of the mean Indian summer monsoon.

Based on the two track data sets just discussed, numerous studies have reported a large decrease in the number of monsoon depressions forming each summer in recent decades, together with an increase in the number of monsoon lows (Prajeesh et al., 2013; Rajendra Kumar & Dash, 2001; Vishnu et al., 2016, and references therein). When characterized as a linear trend, the decrease in depression counts amounts to a reduction of around one per decade, from a midtwentieth century value of about 7, although much of the decrease occurred as a step-wise reduction in the early 1980s (Vishnu et al., 2016). The years 2002, 2010, and 2012 contained the first summers, in over a century of record keeping by IMD, with no monsoon depressions. The reduction in depression counts has been argued to be associated with a decrease in total summer rainfall in east central India, the region of highest LPS track density (Vishnu et al., 2016). A decrease in overall LPS activity, including that of both lows and depressions, has been projected for the coming century as global mean temperature increases and the large-scale, seasonal mean monsoon circulation weakens (Rastogi et al., 2018; Sandeep et al., 2018). This projected decrease is accompanied by a poleward shift in the region of LPS genesis in next-century simulations using one global climate model (Sandeep et al., 2018), but the connection of such greenhouse gas-forced changes to past trends remains unclear, especially given the possible dominance of aerosol forcings in historical trends of mean monsoon strength (Bollasina & Nigam, 2009; Ramanathan et al., 2005).

The existence of a large trend in monsoon depression counts was questioned by Cohen and Boos (2014), who showed that no such trend could be detected in two reanalyses when automated algorithms were used to track and classify low-level vorticity and MSLP anomalies. Furthermore, Cohen and Boos (2014) found depression-strength LPS in those reanalyses during the years when IMD recorded none (2002, 2010, and 2012) and showed that satellite scatterometer data validated the intensity of the peak surface wind speeds near the centers of those particular storms. They also showed that there was no detectable trend in a satellite scatterometer record of synoptic-scale wind events over the Bay of Bengal, although that record extended back to only 1987. All of these raise numerous questions: Are the two reanalyses examined by Cohen and Boos (2014) reliable tools for assessing trends in monsoon LPS, especially given that they extended back to only 1979, a few years before the step-wise reduction in IMD's depression counts? Should we expect trends inferred from the IMD record of depression counts to be unbiased, given the large changes since the late nineteenth century in the observing network, in methods used by IMD for identifying and classifying LPS, and possibly in practices used for creating the hand-drawn IMD weather charts?

All of this would seem to call for a reanalysis of monsoon LPS track data sets, analogous to the large international efforts to improve track data sets of past tropical cyclones (Delgado et al., 2018; Hagen et al., 2012; Landsea et al., 2008, 2014). This would be a massive undertaking, made more difficult by the fact that IMD synoptic charts are not readily available and by the fact that monsoon LPS have weak circulations compared to tropical cyclones. Furthermore, the wind maxima of LPS are typically elevated a few kilometers above the surface (Godbole, 1977), rendering their identification and categorization using maps of MSLP even more difficult. Here we take an alternate approach by devising an algorithm that can identify LPS using elevated winds as well as surface conditions as represented in five atmospheric reanalyses, including the most modern ones that represent climate forcings and that extend back in time to the 1950s. This does not eliminate bias that might be introduced by the temporal evolution of the observing network on which those reanalyses are based, and, indeed, we demonstrate that step-wise changes in depression counts coincide with dates on which geostationary satellite imagery began to be incorporated into the atmospheric state estimates.

This study builds on previous attempts to compile LPS track data sets from reanalyses (Hurley & Boos, 2015; Praveen et al., 2015) but with greater attention paid to the optimality of the tracking algorithm, to uncertainty characterization, to separation of the data sets used for training and validation of the algorithm, and to application of the algorithm to a larger number of reanalyses and to more modern reanalyses. Past efforts to track LPS in atmospheric reanalyses used the TRACK algorithm (Hodges, 1995, 1998; Hurley & Boos, 2015), which runs serially and requires degrading the underlying data set to T42 spectral resolution (Manganello et al., 2019; Thorncroft & Hodges, 2001); both of those characteristics become problematic

Table 1
Details of Reanalysis Data Used in This Study

Data set	Spatial resolution	Temporal resolution	Period	Source
ERA-Interim	0.75° × 0.75°	6 hr	1979–2018	Dee et al. (2011)
JRA-55	1.25° × 1.25°	6 hr	1958–2019	Ebita et al. (2011)
CFSR	0.5° × 0.5°	6 hr	1979–2010	Saha et al. (2010)
MERRA-2	0.625° × 0.5°	3 hr	1980–2019	Gelaro et al. (2017)
ERA5	0.25° × 0.25°	1 hr	1979–2019	Hersbach et al. (2019)

when working with modern atmospheric state estimates which often have horizontal grid spacings of 20–30 km. The algorithm we create for LPS identification builds on the TempestExtremes software (Ullrich & Zarzycki, 2017) and is thus fast, objective, and appropriate for high-resolution and variable grids. We hope to use this algorithm in future work to track monsoon LPS in large ensembles of high-resolution output from numerical weather prediction models and global climate models. In this study, the main focus is on constructing the algorithm, demonstrating its fidelity compared to existing, subjectively analyzed LPS data sets (Sikka, 2006), then examining the historical variability of LPS tracks on interannual and longer time scales.

2. Data and Methods

2.1. Subjectively Analyzed Track Data Sets

We use two subjectively analyzed data sets of LPS tracks and intensities in the northern Indian Ocean. The first was compiled by Sikka (2006) and Mooley and Shukla (1987) and runs from 1888–2003, for the months of June through September. We hereafter refer to this as the Sikka archive. As mentioned in section 1, the Sikka archive is the only subjectively analyzed track data set for South Asia that contains both lows and depressions, and it was compiled by manually identifying minima in maps of MSLP from the IMD and then classifying those minima by intensity. The second data set we use is the total number of depressions forming between June and September from 1891–2019, as recorded by the IMD (https://www.rmcchennaieatlas.tn.nic.in). We also use IMD best track data for depressions for 1982–2018.

2.2. Reanalyses

Five global atmospheric reanalyses are used for this study, with horizontal grid spacings ranging from 0.25–1.25° and temporal resolutions ranging from hourly to 6-hourly (Table 1). The variables used are MSLP, surface wind, surface height, land-sea fraction, and the 850 hPa horizontal wind and relative humidity. All of the reanalyses used here assimilated both satellite and conventional (e.g., surface station and radiosonde) observations that increased in number and type over time, with the greatest growth seen in satellite observations. For example, ERA-Interim, produced by the European Centre for Medium-Range Weather Forecasts (ECMWF), assimilated more than 10^6 daily observations in 1989 and almost 10^7 per day in 2010; the great majority of these, by count, are from satellite, but surface and radiosonde observations from land and ship-based stations are also included, with a reasonable count over South Asia (Dee et al., 2011).

The most recent reanalysis from ECMWF, ERA5, incorporates newly reprocessed observations and input from more recent instruments that were not assimilated into ERA-Interim (Hersbach & Dee, 2016; Hersbach et al., 2019). Similarly, the Modern-Era Retrospective Analysis for Research and Applications, version 2 (MERRA-2) (Gelaro et al., 2017) and the Climate Forecast System Reanalysis (CFSR) (Saha et al., 2010) both assimilate observations not included by their predecessors, with large increases in observation counts in recent decades. In MERRA-2, for example, the number of assimilated aircraft observations increased gradually by a factor of about 4 from the late 1990s to 2015, eventually becoming the dominant source of direct measurements of upper-level winds, while large step-like increases in the number of assimilated satellite radiances occurred in 2002, 2008, and 2013 (McCarty et al., 2016). Since we are interested in the large changes in monsoon depression counts seen in IMD data in the late 1970s and early 1980s, we also use the Japanese 55-year Reanalysis (JRA-55) (Ebita et al., 2011; Kobayashi et al., 2015) which extends back

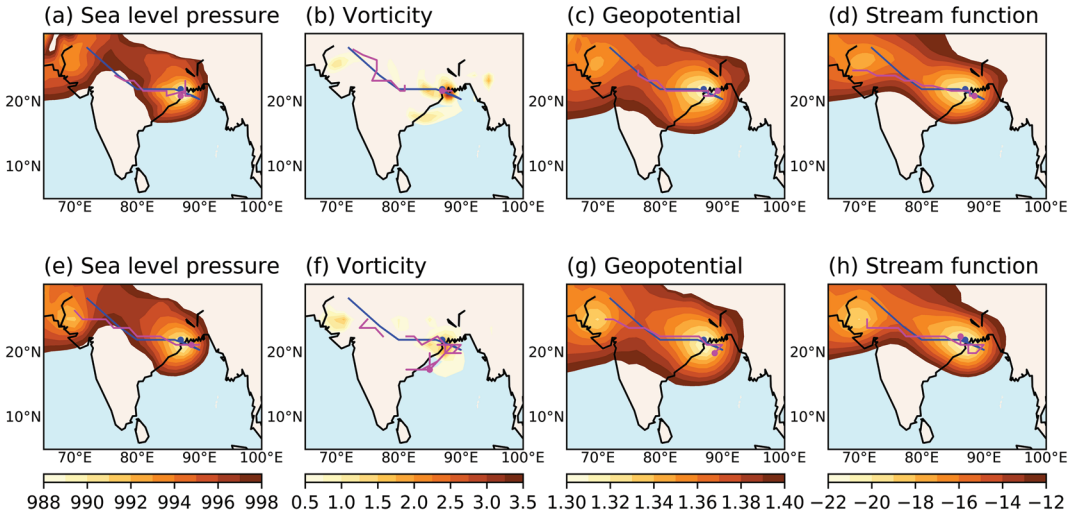

Figure 1. An illustration of LPS tracking using different search variables. The shaded region is (a, e) mean sea level pressure in hPa, (b, f) vorticity at 850 hPa in 10^{-4} s^{-1}, (c, g) geopotential at 850 hPa in 10^{4} m^{2} s^{-2}, and (d, h) stream function at 850 hPa in 10^{6} m^{2} s^{-1} on 26 July 2003 at 00:00 UTC, corresponding to the point of maximum strength during the lifetime of an LPS. The LPS genesis point and track obtained using the given search variable are shown as the magenta dot and line, respectively. The blue dot and line are the Sikka archive LPS genesis point and track, respectively. The top panel shows results from ERA-Interim and the bottom panel from JRA-55.

to 1958. Only conventional observations were assimilated by JRA-55 before 1971, and the greatest increase in the number of assimilated satellite observations occurred after 1979.

Some of the reanalyses we use include time-varying climate forcings that may influence trends in LPS activity. For example, ERA5 incorporates the Coupled Model Intercomparison Project 5 (CMIP5) radiative forcing, accounting in a self-consistent manner for changing greenhouse gases, volcanic eruptions, sea surface temperarture (SST), and sea ice cover (Hersbach & Dee, 2016; Hersbach et al., 2019). This contrasts with ERA-Interim, which imposes a simple linear trend in greenhouse gas concentrations and uses a succession of different SST and sea ice data sets with some temporal discontinuities (Dee et al., 2011). CFSR incorporates time-evolving greenhouse gases, aerosols, and solar variations, while JRA-55 includes time-varying greenhouse gases but a two-dimensional monthly climatology of aerosol optical depth. MERRA-2 uses a sophisticated assimilation of aerosol observations, together with prescribed increases in carbon dioxide.

2.3. Precipitation and SST Data

We employ several additional data sets to create indices used in assessing interannual variations of LPS activity. Indian summer rainfall is obtained from the Indian Institute of Tropical Meteorology (IITM; https://www.tropmet.res.in/Data%20Archival-51-Page) and is used to identify pluvial and drought summer monsoon years. The Oceanic Niño Index (ONI) is used as an ENSO indicator and obtained from the Climate Prediction Center (https://origin.cpc.ncep.noaa.gov/products/analysis_monitoring/ensostuff/ONI_v5.php). Monthly mean SST from the Hadley Centre Global Sea Ice and Sea Surface Temperature version 2 data set (HadISST2)(Rayner et al., 2003) is used to compute the Indian Ocean Dipole (IOD) index; specifically, we use a normalized index represented by the anomalous SST difference between the western (10°S to 10°N, 50–70°E) and eastern (10°S to equator, 90–110°E) Indian Ocean.

2.4. TempestExtremes

An automated Lagrangian pointwise feature tracker, TempestExtremes, is used for extracting LPS track information from the reanalyses (Ullrich & Zarzycki, 2017). TempestExtremes has been used for tracking features including tropical cyclones, extratropical cyclones, and tropical easterly waves (Chavas et al., 2017; Michaelis & Lackmann, 2019; Ullrich & Zarzycki, 2017; Zarzycki, Thatcher, et al. 2017). The basic algorithm uses the MapReduce technique, which operates in two stages: first, parallel identification of suitable candidates at each time step through application of thresholds and/or criteria that enforce a closed contour around the candidate points; second, stitching of nearby candidates over successive time steps to

develop object tracks, eliminating candidates that do not exhibit behavior consistent with a transiting feature. Here, we use the specific requirement that candidate points must be within 3° of each other on successive time points to be linked. If no points exist within 3° of an existing point in the succeeding 12 hr period, then the track is terminated. Because we use this 12 hr period, rather than the time resolution of the input data, for joining successive points into a track, the stitching process is not expected to be highly sensitive to the temporal resolution of the input data.

The criteria for initial identification of suitable candidates explored in this work require identifying features that are local minima or maxima, tagging only the strongest candidate within 5° great-circle distance and testing for a closed contour in a specified search variable of specified magnitude and within a specified distance. The closed contour criterion is assessed via a depth-first search of grid points away from the nodal feature, ensuring that all possible paths away from the feature reaching the prescribed distance exhibit an increase (or decrease) in the search variable of sufficient magnitude. One minor additional modification is made to remove LPS that may appear due to artifacts of the representation of high orography in reanalyses: We require the maximum surface geopotential within 2° of the LPS center to be less than 8,000 $m^2\,s^{-2}$ for at least 24 cumulative hours of the LPS track. That is, LPS that spend nearly their entire lifetime over elevated terrain are are not included in our data set.

Features identified using the above procedure are initially classified as LPS. Monsoon depressions, which are strong LPS, are subsequently classified by requiring a closed contour magnitude of MSLP that is greater than or equal to 4 hPa and a maximum surface wind speed within 3° great-circle distance higher than 8.5 $m\,s^{-1}$ sustained for at least 6 hr along the track, similar to the IMD classification of depressions. LPS that do not satisfy these criteria are categorized as lows.

An LPS tracked using four different search variables is shown in Figure 1. The feature is tracked successfully for all four variables in both ERA-Interim and JRA-55, despite differences in spatial resolution between these data sets. There are differences in the track length compared to the Sikka archive. Visually, tracking performed with stream function, geopotential, and MSLP matches the Sikka track well, whereas tracking performed using vorticity does not, producing a disjointed track in both reanalyses. We systematically evaluate the performance of different tracking variables in section 3.

2.5. Skill Metric

To assess the agreement between LPS tracks obtained from our training data sets (the reanalyses) and the reference data set (the Sikka archive), an event-matching algorithm is employed. Tracks are considered matched between two or more data sets when their points lie within 3° great-circle distance of each other for at least 1 day in their lifetime. The degree of match between tracks in the training and reference data sets is first quantified in terms of a hit ratio and false alarm ratio. The hit ratio is the fraction of matches in the reference data set also detected in a training data set. The false alarm ratio is the fraction of features in a training data set without a match in the reference data set.

We also use the Critical Success Index (CSI) (Di Luca et al., 2015) to assess algorithm skill. This index accounts for both matches and nonmatches using a single skill score,

$$\mathrm{CSI}(\text{data set, reference}) = \frac{\langle \text{matches} \rangle}{\langle \text{matches} \rangle + \langle \text{nonmatches} \rangle}. \tag{1}$$

Here $\langle \text{matches} \rangle$ is the count of matches between a training data set and the reference data set, and $\langle \text{nonmatches} \rangle$ is the average count of nonmatches in the training and reference data sets.

Since the reference data set (the Sikka archive) may contain errors, it is inadequate to simply choose a tracking algorithm that maximizes the CSI for this single reference data set. Hence, we also consider the degree to which a track is represented similarly across all reanalyses. We create a combined CSI that weights agreement between all of the reanalyses with agreement between the reanalyses and the Sikka archive,

$$\mathrm{CSI}_{combined} = \frac{\mathrm{CSI}_{EJCM} + \dfrac{\mathrm{CSI}_{ES} + \mathrm{CSI}_{JS} + \mathrm{CSI}_{CS} + \mathrm{CSI}_{MS}}{4}}{2}. \tag{2}$$

Here CSI_{EJCM} is the CSI among all four reanalyses—namely, considering ⟨matches⟩ to be the count of LPS common in all four reanalyses and ⟨nonmatches⟩ to be the average of nonmatches among all four reanalyses. In the latter case, we define a nonmatch as occurring in a particular reanalysis when the LPS detected in that reanalysis is not identified in at least one other reanalysis. The terms CSI_{ES}, CSI_{JS}, CSI_{CS}, and CSI_{MS} are the four CSI values of the four individual reanalyses (ERA-Interim, JRA-55, CFSR, and MERRA-2, respectively) compared with the Sikka archive. The combined CSI is employed to rank the performance of each tracking algorithm.

3. An Optimized Tracking Algorithm

Since monsoon lows and depressions have weaker intensities than classic tropical cyclones, it has been a challenge to detect and classify these LPS in reanalyses. A variety of methods have been used for this task, with relatively low levels of agreement between the resulting track data sets. For example, Hurley and Boos (2015) and Hunt et al. (2016) both identified LPS as cyclonic extrema of lower tropospheric relative vorticity having concurrent negative anomalies of MSLP relative to a 21-day mean. Those studies used only ERA-Interim data. Praveen et al. (2015) identified LPS in both ERA-Interim and MERRA with a detection algorithm designed to mimic the manual identification of LPS performed by IMD, thus using only MSLP. Even when mimicking the traditional detection methodology, Praveen et al. (2015) obtained only modest correspondence with the Sikka archive: Correlation coefficients for interannual variations of monsoon LPS counts were 0.4 and 0.5 for ERA-Interim and MERRA, respectively, referenced to the Sikka archive. All of the above studies chose thresholds (e.g., a 2 hPa MSLP anomaly) for their detection algorithms based on some combination of physical understanding and traditional identification methods, with little systematic assessment of those thresholds.

3.1. Candidate Variables and Thresholds

Here we assess multiple candidate variables and detection thresholds to obtain a tracking algorithm that is more nearly optimal across multiple reanalyses. Although it is possible that every reanalysis and every particular configuration of an atmospheric model will have a unique geophysical variable and set of thresholds that allow LPS identification to best match traditional methods (e.g., those used by IMD), retuning tracking algorithms in this way is undesirable from the perspectives of both practicality and scientific understanding. So we perform a sensitivity analysis using a set of candidate variables, with ranges of corresponding thresholds and the skill metric defined above (the CSI).

We include MSLP and the 850 hPa relative vorticity (ζ) in this set of candidate variables because these have previously been used for tracking monsoon LPS and, more generally, tropical cyclones (for a relevant history see Bengtsson et al., 1982; Broccoli & Manabe, 1990, and Appendix B of Ullrich & Zarzycki, 2017). Drawbacks exist for both of those variables, with peak values of vorticity depending on the horizontal resolution of the underlying data set, and MSLP being only an indirect indicator of the circulation several kilometers above the surface, where monsoon LPS typically have strongest winds. For this reason, we also consider the 850 hPa geopotential, which provides the geostrophic circulation closer to the level of strongest winds. Additionally, we consider the stream function (ψ) of the horizontal wind; through the relation $\nabla^2\psi=\zeta$, it has an exact relation to the relative vorticity but is much smoother than that variable. The geopotential and MSLP are similarly related to the vorticity only under conditions of low Rossby number, and monsoon depressions can easily achieve Rossby numbers of 2 (Boos et al., 2015). A practical challenge exists when computing ψ on a level of a vertical coordinate system that intersects the ground, because boundary conditions must be imposed on that intersection when inverting the winds (or vorticity) to obtain the stream function. Some reanalyses (e.g., ERA-Interim) extrapolate winds beneath Earth's surface, and we choose to replace those extrapolated values with 0 prior to inverting ζ to obtain ψ. More discussion of issues involved in calculating the stream function is provided in Appendix A. In summary, the set of variables used to create candidate tracking algorithms are MSLP, 850 hPa relative vorticity, 850 hPa geopotential, and 850 hPa stream function (see also Table 2). We later test the sensitivity of the chosen geophysical variable to the choice of vertical level.

Detection of LPS involves using TempestExtremes to locate minima of MSLP, geopotential, or stream function, or maxima of vorticity, then testing whether that extremum is surrounded by a closed contour of the same field within a specified radius. This effectively tests the magnitude of the radial gradient, relative to

Table 2
Variables and Closed Contour Magnitudes Used for Detecting Low-Pressure Systems

Search variable	Closed contour magnitudes
Mean sea level pressure (Pa)	25, 50, 75, 100, 125, 150, 175, 200
Geopotential at 850 hPa ($m^2\ s^{-2}$)	25, 50, 75, 100, 125, 150, 175, 200
Stream function at 850 hPa ($10^5\ m^2\ s^{-1}$)	5.0, 7.5, 10.0, 12.5, 15.0, 17.5, 20.0, 25.0
Relative vorticity at 850 hPa ($10^{-5}\ s^{-1}$)	2.5, 3.0, 3.5, 4.0, 4.5, 5.0, 5.5, 6.0

a local extremum, in a given variable, making the algorithm insensitive to trends in the horizontal mean of that variable. Use of the closed contour criterion reduces the sensitivity of the method to resolution and furthermore resembles traditional methods, as discussed above. See Ullrich and Zarzycki (2017) for details on how TempestExtremes implements the closed contour criterion. We test eight closed contour magnitudes and two radii for identifying extrema, with the closed contour magnitudes and radius together essentially specifying a minimum radial gradient that must exist for the extremum to be classified as an LPS. We use radii of 5° and 10° of great circle distance, with the eight closed contour magnitudes for each candidate variable shown in Table 2. This approach is analogous to that used by Zarzycki and Ullrich (2017) in developing optimal criteria for identification of tropical cyclones using TempestExtremes.

We additionally desire a criterion for distinguishing LPS from "heat lows," which are nonprecipitating low-pressure systems trapped in the lower troposphere (Ramage, 1971; Rácz & Smith, 1999). Heat lows frequently form over northwestern India during summer and over central India before monsoon onset there; they fulfill all the traditional kinematic criteria for LPS discussed in section 1 but seem to be traditionally excluded from LPS data sets by some implicit criteria that we suspect involves their geographic location or moisture content. We initially attempted to use a precipitable water criterion to distinguish heat lows from traditional LPS but recognized that the increase in precipitable water expected in a warming climate might create spurious trends in LPS counts. One alternative would be to require a minimum precipitation rate to distinguish heat lows from LPS, motivated by the fact that most interest in LPS exists because of their heavy precipitation. But precipitation rates have large variance on short time and space scales and are also subject to trends in a warming climate. So we opt to distinguish LPS from heat lows using the 850 hPa relative humidity (RH), averaged within 3° of the LPS center. Eight RH thresholds ranging from 55% to 90%, with an interval of 5%, are used in the candidate tracking algorithms. The RH is required to exceed these thresholds for a cumulative period of at least 1 day over the disturbance lifetime to be considered an LPS; otherwise it is categorized as a heat low. This choice thus includes systems in our LPS data set that spend much of their lifetimes as nonprecipitating, low-RH disturbances but that achieve high lower-tropospheric RH for at least 1 day.

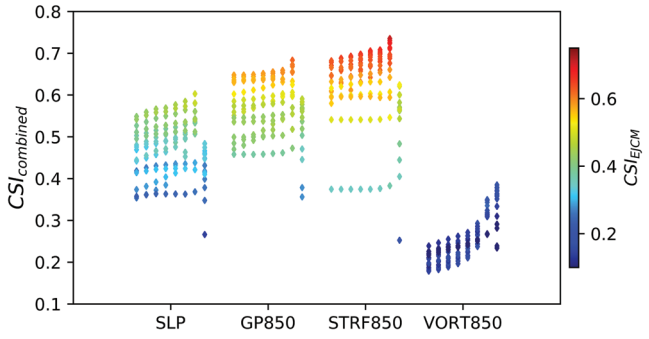

Figure 2. Illustration of the greater skill of 850 hPa stream function in detecting LPS. Each diamond marks the combined Critical Success Index (defined in text) for one combination of closed contour magnitude, radius, and relative humidity (RH) threshold. Shading represents consistency of the algorithm across reanalyses. The tested variables were mean sea level pressure (SLP), 850 hPa geopotential (GP850), stream function of the 850 hPa horizontal wind (STRF850), and 850 hPa relative vorticity (VORT850). Each column within a variable represents one RH threshold, from 55% (left) to 90% (right) with an interval of 5%.

3.2. Assessing Candidate Tracking Schemes

Using the above sets of candidate variables, closed contour magnitudes, radii, and RH criteria, we use TempestExtremes to identify LPS in four reanalyses (ERA-Interim, JRA-55, CFSR, and MERRA-2; see Table 1) for the training period of 1990–2003. This 14-year training period is chosen to overlap with the Sikka archive, which ends in 2003, while leaving a substantial period for verification (1979–1989). A total of 2,048 track data sets are thus created (4 reanalyses × 4 candidate variables × 8 closed contour magnitudes × 2 radii × 8 RH thresholds).The maximum surface wind speed within 3° of the center is used as the maximum sustained surface wind speed of a storm at a time step, and is used later to classify disturbances as lows and depressions. The land-sea ratio of the grid point at the center of each LPS is used for region-wise categorization, with storms treated as being over land when this ratio is higher than 0.5. The TempestExtremes commands for tracking LPS using these criteria are provided in Appendix B.

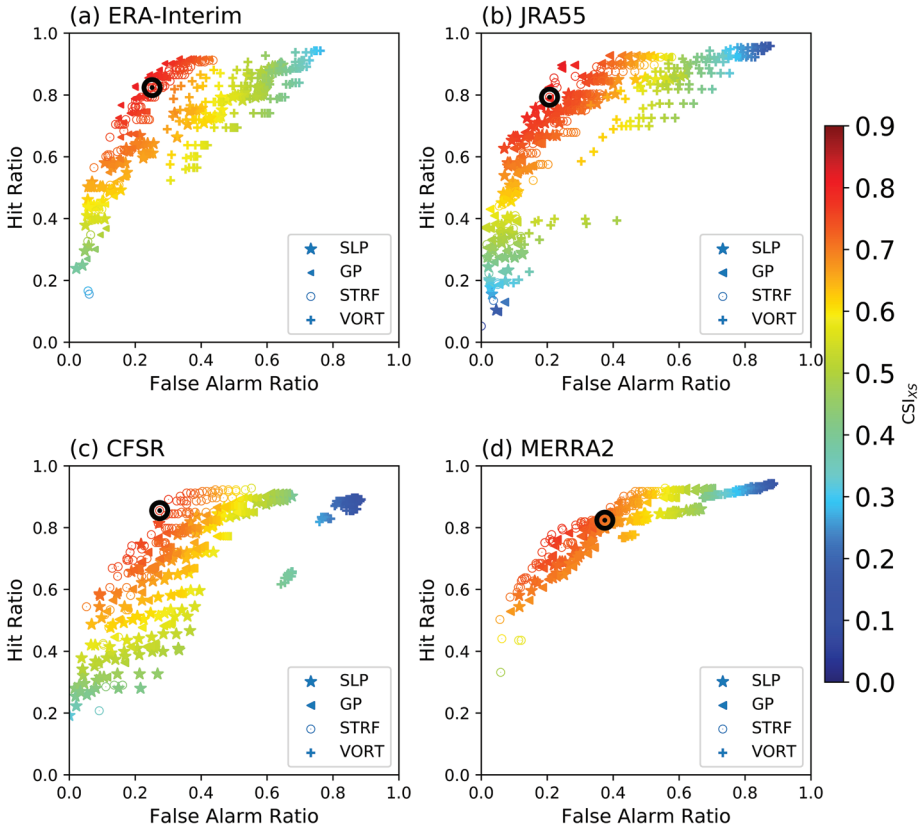

Figure 3. Hit ratio versus false alarm ratio (see text for definition) with respect to the Sikka archive for all LPS algorithms, shaded by CSI_{XS} for (a) ERA-Interim, (b) JRA-55, (c) CFSR, and (d) MERRA-2. The black circle represents the selected optimal algorithm (top-ranked by the combined CSI).

We perform a sensitivity analysis by ranking the 512 tracking algorithms, for each of the four reanalyses, by the combined CSI (Figure 2). As described in the previous section, the combined CSI is a weighted average of the agreement of each reanalysis track data set with the Sikka archive and the agreement between all reanalyses. The top 31 algorithms by this ranking all use the 850 hPa stream function. The top-ranked algorithm requires a disturbance to have an 850 hPa stream function that increases by 1.25×10^6 from the center minimum within a radius of 10°, while achieving an 850 hPa RH of at least 85% for at least 1 day. The second-best variable for tracking LPS is the 850 hPa geopotential (closed contour magnitude of 125 $m^2\ s^{-2}$ and RH higher than 85%). The lower ranking (32 out of 512) of the geopotential comes mainly from greater disagreement between reanalysis tracks, that is, a smaller value of CSI_{EJCM} in Equation 2, and algorithms based on geopotential are only slightly less skillful than those based on stream function (Figure 2). Since stream function is not included in most reanalyses and must be computed prior to running the tracking algorithm, the geopotential is a viable alternative for LPS tracking that requires only a slight compromise in skill. Algorithms based on MSLP have lower skill, with the highest rank of 133 (out of 512); the lower rank comes mainly from greater disagreement between reanalyses but with some contribution from disagreement with the Sikka archive (not shown). The least skillful algorithms all use the 850 hPa vorticity, with the highest rank of 359 out of 512. The vorticity-based algorithms produce track data sets that disagree most strongly between reanalyses and that differ most with the Sikka archive. This is notable given the number of past studies that have used vorticity or potential vorticity to track synoptic-scale monsoon disturbances in Asia, Africa, and Australia (Berry et al., 2012; Hunt et al., 2016; Hurley & Boos, 2015; Thorncroft & Hodges, 2001). Variables and thresholds for the top five ranked algorithms and the top algorithm of each search variable are depicted in supporting information Table S1.

Although the consistency of an algorithm across reanalyses constitutes a large part of its skill score, the top-ranking algorithm also captures more than 80% of LPS in the Sikka archive, our reference data set.

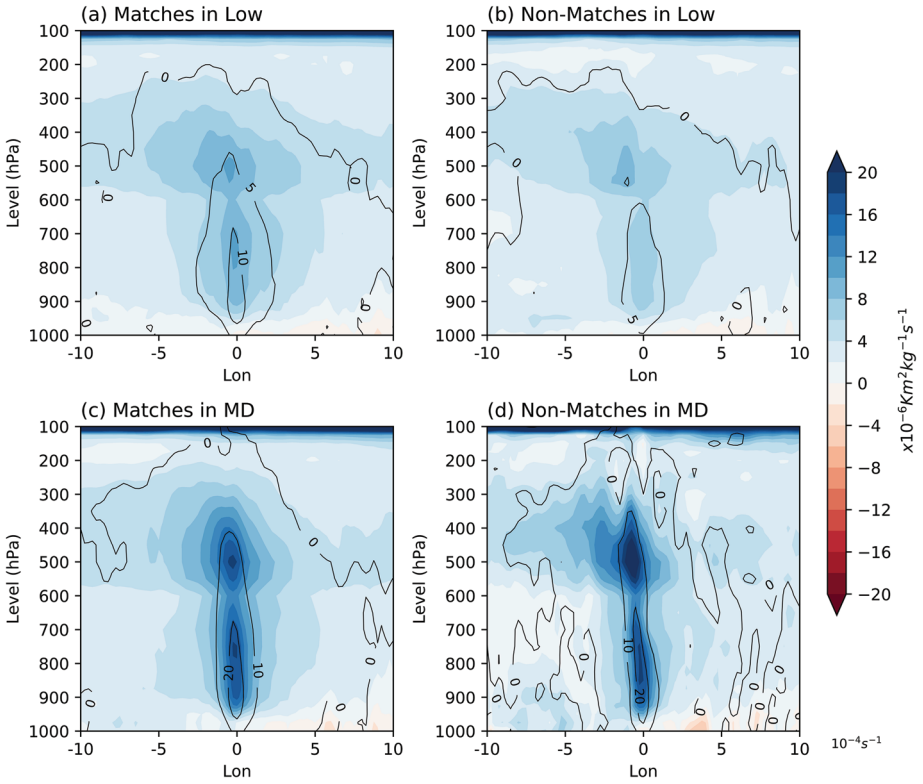

Figure 4. Composite of the vertical cross section of potential vorticity (shaded) and relative vorticity (contours), through the central longitude of the system, for (a) matches in lows, (b) nonmatches in lows, (c) matches in depressions, and (d) nonmatches in depressions.

The fraction of LPS in the Sikka archive that are detected in reanalyses (the hit ratio) is plotted against the fraction of LPS detected in reanalyses that do not exist in the Sikka archive (the false alarm ratio) in Figure 3. Tracking algorithms using the 850 hPa stream function and 850 hPa geopotential have higher CSI values with higher hit ratios and lower false alarm ratios in all reanalyses. In most reanalyses, algorithms based on MSLP have smaller hit ratios than those based on stream function or geopotential. Vorticity-based algorithms have lower CSI values mainly due to higher false alarm ratios in all reanalyses. The top-ranked algorithm by the combined CSI (marked by black circles in Figure 3) compares well with the Sikka data set in all reanalyses, with hit ratios of about 0.8 and false alarm ratios around 0.3.

We also compute the skill scores outside the training period (in the validation period of 1979–1989), finding that there is little change in the level of agreement between each reanalysis and the Sikka archive; the CSI of ERA-Interim, JRA-55, CFSR, and MERRA-2 are 0.79, 0.80, 0.79, and 0.71, respectively, in the training period and 0.78, 0.78, 0.77, and 0.72, respectively, in the validation period. Remarkably, ERA5, which was not used for training, has a higher CSI (0.83), a higher hit ratio, and a lower false alarm ratio than the other reanalyses. This is true despite the fact that ERA5 has hourly, 0.27° resolution while the reanalyses used for algorithm training have grid spacings coarser by factors of 2–6.

For completeness, we also checked whether combining MSLP and 850 hPa vorticity might improve the tracking algorithm, since previous studies used such combinations of variables (Hunt et al., 2016; Hurley & Boos, 2015). Algorithms using a combination of MSLP and vorticity had CSI values around 0.6, similar to those based on MSLP alone. Furthermore, combining stream function and vorticity did not noticeably improve the skill scores. Finally, we tested whether the skill score would improve by using a variable from a different vertical level. Using the stream function of horizontal wind at 1,000, 700, and 500 hPa yielded CSI values lower than those obtained for the 850 hPa stream function.

Using the top-ranked algorithm, we track LPS in all available years of all reanalyses (Table 1). This includes ERA5, which was not used for training.

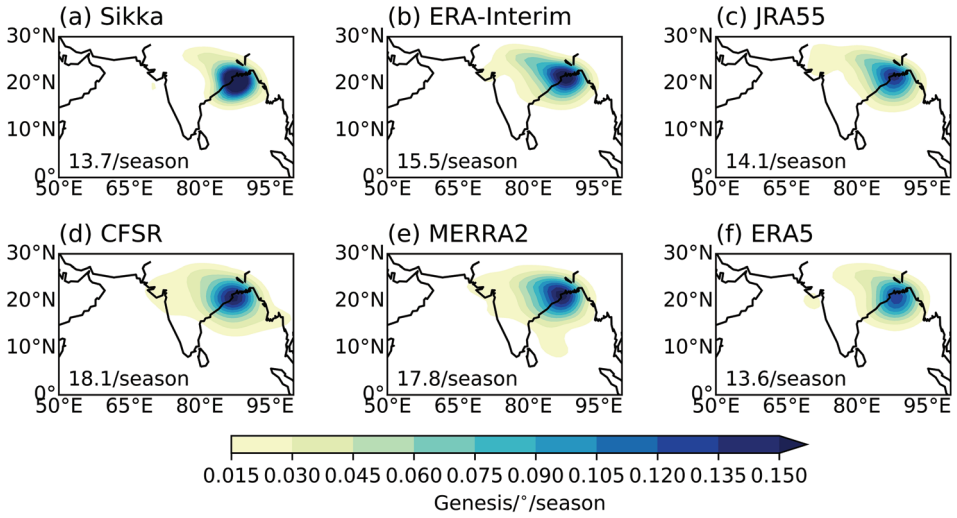

Figure 5. Genesis density of LPS for the period of 1980–2003 in the Sikka archive and reanalyses. Kernel density estimates are used to calculate the genesis density. Numbers in the bottom left corner represent the mean number of LPS in a season for the period. (a) Sikka, (b) ERA-Interim, (c) JRA-55 (d) CFSR, (e) MERRA, and (f) ERA5.

3.3. Are Nonmatches Real Systems?

We now check whether the "false alarms"—LPS identified in reanalyses by our top-ranking algorithm but missing in the Sikka archive—exist due to some error or artifact in the tracking algorithm. We do this by comparing composites of the structures of reanalysis LPS that match those in the Sikka archive with composites of those missing from the Sikka archive. We do this separately for monsoon lows and monsoon depressions, since the implications of a false alarm are different when the LPS is a weak LPS compared to a strong one. We furthermore only include a reanalysis LPS in our composites of false alarms when it is completely missing from the Sikka archive, as opposed to when it is categorized differently (e.g., here we ignore LPS that are classified as a depression in a reanalysis but a low in the Sikka archive). These composites are made using ERA5, since that reanalysis was not used in tuning the tracking algorithm. There are 57 lows and 10 depressions in ERA5 that are missing from the Sikka archive. Composites are created by averaging, in a storm-centered reference frame, the three time steps having the largest central MSLP anomaly.

The composites of lows and depressions have structures consistent with those seen in prior studies (Godbole, 1977; Hurley & Boos, 2015), and these exhibit relatively little differences between matches and nonmatches (Figure 4). The LPS all consist of a column of cyclonic potential vorticity (PV) that extends from the surface to the upper troposphere, with primary maxima near 500 hPa and secondary peaks around 850 hPa. The composite relative vorticity is more bottom-heavy, peaking near 800 hPa. Both the PV and relative vorticity tilt slightly westward with height and are stronger in depressions than in lows, as expected. For lows, the nonmatches (i.e., those present in ERA5 but missing from the Sikka archive) are weaker than the matches, perhaps because the 850 hPa stream function in ERA5 represents weaker systems than were contained in the MSLP maps on which the Sikka archive was based, or perhaps because our tracking algorithm was better able to detect weak systems than the subjective analysis used by the Sikka archive. There is no clear difference between the composites of matching and nonmatching depressions, with any quantitative differences in magnitude likely not significant considering the low number (10) of nonmatches. Comparisons of composites of winds, relative humidities, and temperatures yielded similar results (not shown).

We furthermore obtained the daily MSLP charts from the IMD, which are thought to be similar to those on which the Sikka archive was based, and manually inspected these to search for the 10 depressions present in ERA5 but missing in the Sikka archive. At the times and locations of all 10 of these missing depressions, we found LPS-like features in the pressure charts, with three of the charts clearly showing disturbances marked on the charts as depressions or a more intense category of LPS. We conclude that the 10 additional depressions in ERA5 are real and were somehow missed when the Sikka archive was created.

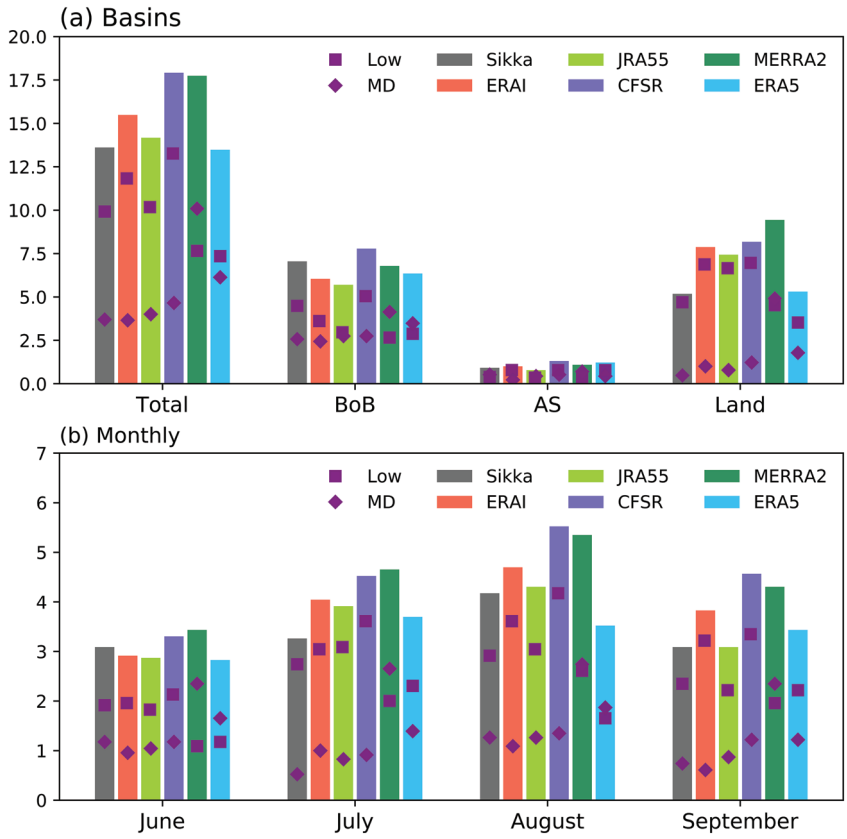

Figure 6. (a) The summer monsoon season (June–September) climatology, for the Sikka archive and reanalyses, of the number of LPS formed over the north Indian Ocean basin and subregions of the Bay of Bengal (BoB), Arabian Sea (AS), and Indian land mass (Land). (b) Climatological monthly variation of LPS. Monsoon lows and monsoon depressions are represented as squares and diamonds, respectively. The period of analysis is 1980–2003.

4. Assessing the LPS Climatology in Reanalyses

We now examine the climatological mean distributions of genesis density, track density, disturbance lifetime, and track length, with the goal of assessing whether the overall statistics of disturbances identified in reanalyses agree with the well-known statistics of monsoon LPS.

4.1. Genesis

The boreal summer (June–September) distributions of genesis frequency for all LPS are broadly similar among all reanalyses and the Sikka archive (Figure 5). The latter has genesis more concentrated over the northern Bay of Bengal, but with a total number of LPS—14 per summer—similar to that in most of the reanalyses. The total count is higher in MERRA-2 and CFSR, around 18 per summer.

There is general agreement among the reanalyses, and between the reanalyses and the Sikka archive, regarding the partitioning of LPS into lows and depressions, the rate of genesis over land compared to that over ocean, and the seasonal cycle of genesis (Figure 6). The most notable outlier is MERRA-2 which, unlike the other four reanalyses and the Sikka archive, has more depressions than lows.

Consistent with the spatial distributions of genesis shown in Figure 5, most reanalyses also represent a larger fraction of LPS forming over land, compared to the Sikka archive (Figure 6). ERA5 has the fewest LPS of all the reanalyses, though the difference is relatively small, and the ERA5 total count is an almost exact match to the Sikka archive. The match with the Sikka archive is notable because ERA5 was not included in the algorithm's training data set. All the reanalyses also capture the greater frequency of LPS in the middle of summer, although ERA5 shows slightly greater frequency in July while all other reanalyses and the Sikka

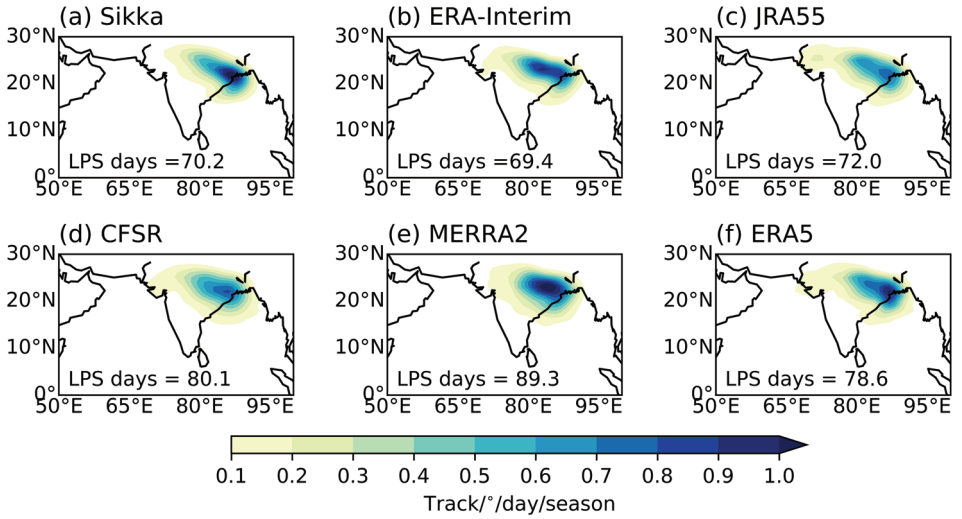

Figure 7. Track density of LPS for the period of 1980–2003 in the Sikka archive and reanalyses. Kernel density estimates are used to calculate the track density of LPS. Numbers in the bottom left corner represent the mean number of days in which LPS are present in a season for the period. (a) Sikka, (b) ERA-Interim, (c) JRA-55 (d) CFSR, (e) MERRA, and (f) ERA5.

archive show greatest frequency in August. This seems to be an improvement over previous reanalysis-based tracking algorithms, which showed genesis occurring more frequently in June than in August in ERA-Interim (Hurley & Boos, 2015).

4.2. Track Density and Lifetime of LPS

All the reanalyses show a similar track density distribution to that seen in the Sikka archive, although the reanalyses extend further westward toward northwestern India (Figure 7). The highest track density over land is found in MERRA-2; that reanalysis also has the highest number of days with an LPS present, which is due to both the high genesis frequency and high LPS lifetime in MERRA-2 (Figure 8).

Lifetimes are generally longer in the reanalyses, with the longest found in ERA5, which has LPS lasting one to 2 days longer than the Sikka archive. The distributions of lifetimes for all LPS are more strongly skewed in the reanalyses than in the Sikka archive, with the median lifetime being almost a full day shorter than the mean lifetime (Figure 8a). Track lengths (in great circle distance between start and end points) are similar between the reanalyses and Sikka archive, implying a slower translation speed in the reanalyses: 2.3 m s^{-1} in the Sikka archive and 1.6–1.91 m s^{-1} in the reanalyses. In all data sets, depressions have longer tracks and lifetimes than lows, and tracks and lifetimes are longer over ocean than over land.

5. Interannual and Long-Term Variations

5.1. Interannual Correlations Between Data Sets

The interannual variability of seasonal total counts of LPS, lows, and depressions has a similar magnitude across reanalyses and the Sikka archive, but these variations exhibit low to modest correlation between data products (Figures 9a–9c). The correlations between different reanalyses of seasonal LPS counts range from about 0.5 to 0.75, higher than the 95% confidence level of 0.34 for this sample size, with the two ECMWF reanalyses being most strongly correlated. Interannual correlations between data sets are weaker for the individual categories of lows and depressions (Figures 9b and 9c); this is not surprising since differences in the categorization of an LPS as a low versus a depression can arise from small differences in surface pressure and wind speed. Any negative correlations exist only for these subcategories (e.g., between depression counts in JRA-55 and the Sikka archive; Figure 9c) and are not statistically significant. The data set having the weakest correlations with all others is the Sikka archive; the LPS data set of Hurley and Boos (2015) also showed little interannual correlation with the Sikka archive. This might arise due to differences in the geophysical observations on which each data set is based, on the variables used for tracking, and on other

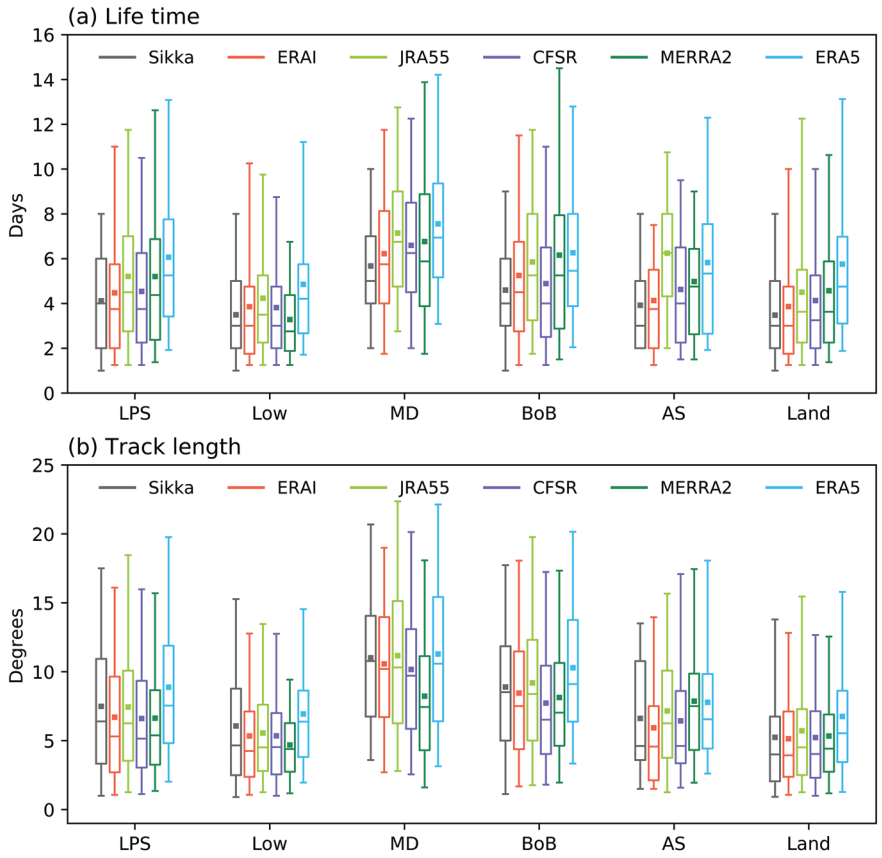

Figure 8. Box-and-whisker plots of (a) lifetime and (b) track length of LPS in Sikka archive and all reanalyses. The horizontal line within the boxes indicates the median, boundaries of the boxes indicate the 25th and 75th percentiles, the whiskers indicate the 5th and 95th percentile values, and the solid square represents the mean value. The period of analysis is 1980–2003.

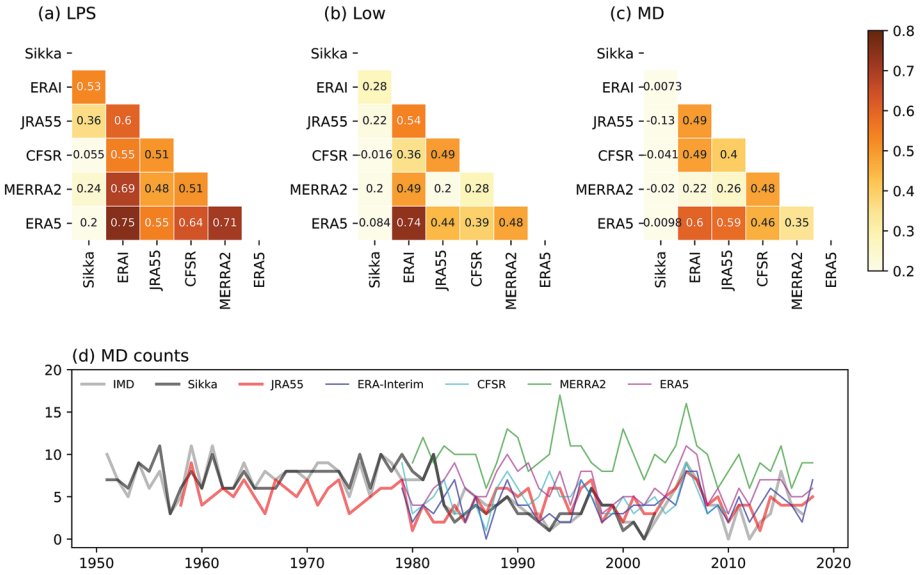

Figure 9. Interannual correlation of the number of Indian summer (June–September) (a) monsoon low-pressure systems, (b) lows, and (c) depressions between the data sets, including the Sikka archive and the reanalyses during 1980–2003, the years in which all LPS data sets are available. (d) Year-to-year variation in the number of monsoon depressions in all reanalysis data sets, the Sikka archive, and the IMD data set.

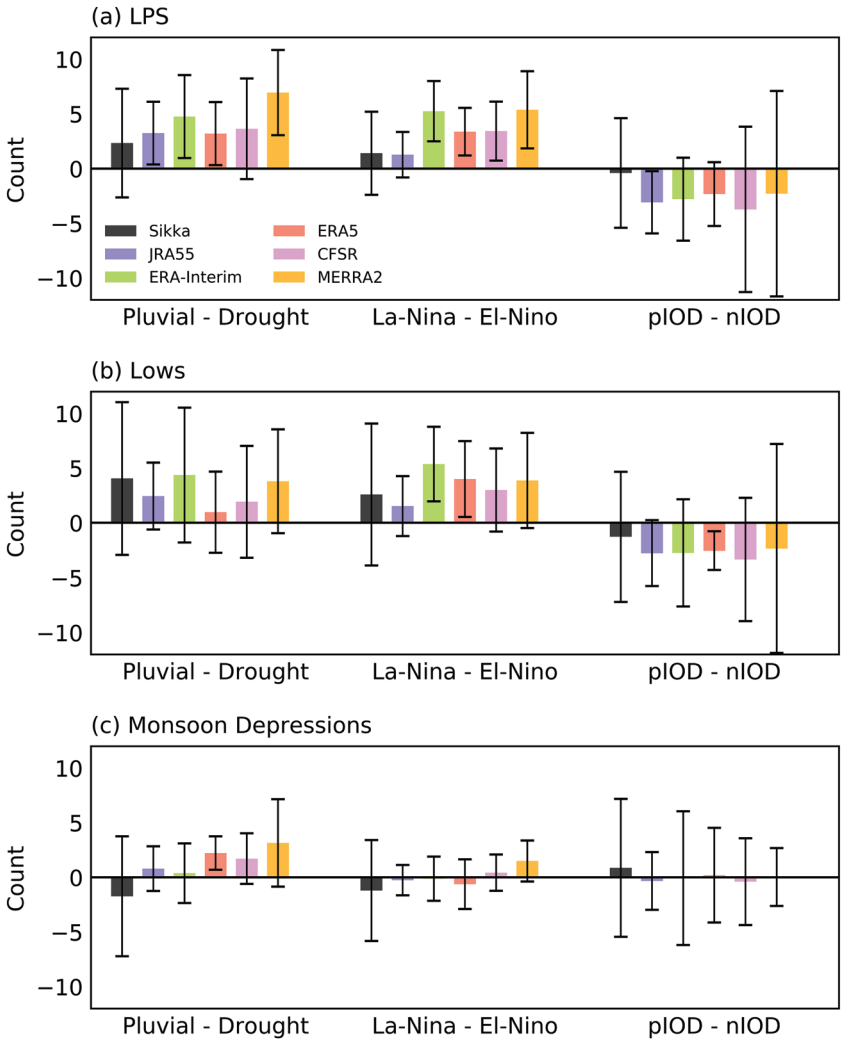

Figure 10. Difference of (a) LPS, (b) low, and (c) depression mean counts in pluvial-drought summer monsoon years, La Niña-El Niño years, and positive-negative Indian Ocean Dipole years. The vertical lines represent the 95% confidence interval for the difference in the mean counts. Analysis of each data set includes all available periods of that data set (see Table 1).

methodological details. In particular, LPS in the Sikka archive were identified through manual analysis of surface pressure charts, which were in turn obtained through manual analysis of station observations; such subjective methods might introduce random and/or systematic errors (e.g., a bias toward identifying LPS over land).

We now explore the differences that reduce interannual correlations between data sets, using brief statistical modeling to explain how the modest correlations seen in Figure 9 are consistent with the seemingly good skill scores shown in Figure 3. We state in section 3.3 that 67 LPS are present in ERA5 but not in the Sikka archive; these nonmatching storms, which account for about 20% of the total number of storms in the record, reduce the interannual correlation between those two data sets. We test the sensitivity of the interannual correlations to missing storms by removing random LPS from the Sikka archive between 1979 and 2003, adding the same number of "false alarm" LPS to random years in that archive, then recalculating the interannual correlation with the original Sikka archive. Removing 67 random storms and adding the same number of false alarms degrades the correlation coefficient from 1.0 to an average of 0.62 (with a 95% confidence interval of 0.36–0.81, empirically sampled from 5,000 iterations). Increasing the fraction of randomly replaced storms to one third of those in the Sikka archive further degrades the correlation

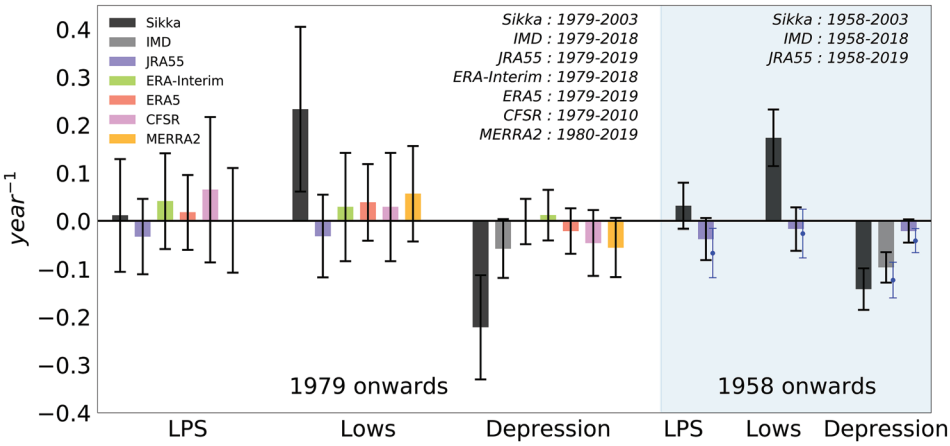

Figure 11. Linear trends in LPS, lows, and depressions in the Sikka archive and reanalyses. The white shaded region shows trends from 1979 onward, while gray shaded region shows trends from 1958 onward. Error bars represent the 95% confidence interval for these trends. Blue dots and error bars represent the trend and 95% confidence interval, respectively, for the extended season of May to October. The 95% confidence intervals assume a normal distribution and thus are 1.96 times the standard error.

coefficients, in this statistical model, so that the 95% confidence interval is 0.08–0.7, encompassing the correlations between the Sikka archive and most reanalyses. Thus, the relatively low interannual correlation each reanalysis has with our reference data set is consistent with the hit ratios and false alarm ratios seen in Figure 3. We note that the interannual correlation between the Sikka archive and ERA-Interim (0.53) is higher than reported by Praveen et al. (2015) (0.2 to 0.4); those authors detected LPS using surface pressure, which we show in section 3.2 produces worse skill than detectors based on stream function (which was used in the tracking algorithm examined here).

In summary, the interannual correlation between two data sets can be greatly reduced when a modest fraction of storms in one data set does not match the other data set. Our statistical modeling showed that replacing 20–30% of the storms in one data set with the same number of randomly distributed false alarms can reduce the correlation coefficient to the levels of 0.2–0.5 frequently seen in Figure 9. Thus, even though the reanalyses capture about 80% of LPS in the Sikka archive, we should not expect the interannual correlations between these data sets to be large. Correlations for the subcategories of lows and depressions will be further reduced by the fact that one in three depressions in the Sikka archive is categorized as a low in the reanalyses and vice versa. Yet there is clearly some agreement: All data sets, including the Sikka archive, capture the high number of depressions in 2006 (Figure 9d), which coincides with an Indian Ocean Dipole event (Krishnan et al., 2011).

5.2. Relation to Interannual Climate Modes

Given the large contribution of LPS to India's total summer rainfall (Yoon & Chen, 2005), some studies have explored whether interannual variations in LPS activity are associated with interannual variations in total Indian summer rainfall (Krishnamurthy & Ajayamohan, 2010; Sikka, 2006). We build on this by analyzing how LPS count, mean lifetime, and track length vary between pluvial and drought years in the Sikka archive and reanalyses. We define “pluvial” years as years when seasonal total rainfall is more than one standard deviation above the mean, and “drought” years as those when rainfall is more than one standard deviation below the mean. LPS counts are significantly higher in pluvial than drought years in four out of five reanalyses (Figure 10a), but there are no significant changes in lifetime and track length in four of five reanalyses (Figures S1a and S2a). Although the Sikka archive shows no change in LPS counts between pluvial and drought years between 1979 and 2003, Krishnamurthy and Ajayamohan (2010) performed the same analysis of the Sikka archive for 1901–2003 and found a higher number of LPS and a higher number of days with LPS conditions in pluvial compared to drought years. When examining how counts of the individual categories of lows and depressions change between pluvial and drought years, most reanalyses and the Sikka archive show no detectable signal (Figures 10b and 10c). The rainfall produced by depressions is higher in pluvial

than in drought years, with the seasonal rainfall accumulation occurring within 8° of an LPS center over Indian land regions differing by 104 ± 96 mm for ERA5 tracks and ERA5 precipitation. For lows and for all LPS, the 95% confidence interval on the difference between pluvial and drought years includes 0 (Figure S3). Performing this analysis with other rainfall products and reanalysis data sets is deemed outside the scope of this study.

Interannual variation of the Indian summer monsoon is highly linked to ENSO, with an increased propensity for drought years in the warm phase of ENSO (El Niño) and pluvial years in its cold phase (La Niña). We find that LPS counts are higher in La Niña years than El Niño years (Figure 10a), and the differences are significant in all data sets except the Sikka archive and JRA-55. When assessing ENSO-related variations in lifetimes and track lengths, the only detectable signal is in ERA-Interim and ERA5, which exhibit LPS lifetimes that are higher in El Niño years than La Niña years (contrasting with their lower average counts in those years; Figure S1a). The fact that a signal is sometimes detected in only one or two out of six data sets shows that it may be important to reexamine results from prior studies that relied on a single data set. For example, Krishnamurthy and Ajayamohan (2010) used only the Sikka archive when showing that LPS activity is roughly equal in El Niño and La Niña years. Hunt et al. (2016) relied on only ERA-Interim when finding that depression activity is 16% higher in El Niño than La Niña years.

Finally, we examine covariations of LPS with the IOD, an SST pattern associated with variations in Indian summer monsoon circulation and rainfall (Saji et al., 1999; Webster et al., 1999). Krishnan et al. (2011) found that depressions have higher track lengths in positive IOD years, and Hunt et al. (2016) found that depression lifetime is 12% higher in positive IOD years. We find that only one reanalysis (JRA-55) shows a change in LPS counts between positive and negative IOD years (Figure 10a), and another reanalysis (CFSR) shows longer depression lifetimes (Figure S1c). For all other data sets, the 95% confidence interval on the IOD-related changes in counts, lifetimes, and track lengths includes 0.

5.3. Trends in LPS

5.3.1. Linear Trend Analysis

Based on the Sikka archive and the IMD data set of depression counts, previous studies discussed an apparent increase in the number of lows and a decrease in the number of depressions forming each summer (Jadhav & Munot, 2009; Prajeesh et al., 2013; Vishnu et al., 2016, and references therein). However, Cohen and Boos (2014) questioned the existence of a decrease in the number of depressions in the past 40 years, based on their finding that no trend in depression counts could be detected in ERA-Interim and on their discovery of depressions in that reanalysis that were missing in the IMD data set. Here we examine whether a trend in the number of LPS overall, or in the number of lows or depressions, can be detected in any of the track data sets created using our tracking algorithm. We first assess the period since 1979, since four of our reanalyses start in that year, then compare to results starting in 1958 (for which only JRA-55, the Sikka archive, and the IMD data set provide values).

Consistent with previous studies, the Sikka archive shows no trend in the seasonal counts of all LPS since 1979, together with an increasing trend in lows and a decreasing trend in depressions (Figure 11). Any decreasing trend in depression counts in the IMD data set is weaker and has an error bar that includes 0. None of the reanalyses show any appreciable trend in the counts of lows or depressions. Similarly, no significant trend in the total seasonal rainfall produced by LPS, lows, or depression is seen when using ERA5 tracks with ERA5 precipitation (Figure S4); similar trend analyses using other rainfall products will be undertaken in separate work.

Vishnu et al. (2016) noted that the trend in depressions is not linear, but consists mainly of a large reduction around 1980, which lies at the beginning of the records discussed in the previous paragraph. Since JRA-55 is the only reanalysis with data prior to 1979, we compute the trend in depressions for the more extended period starting from 1958 in JRA-55 and compare this with trends from the IMD and Sikka data sets (Figure 11). The IMD and Sikka data sets show depression counts decreasing at a rate of -0.096 and -0.14 year^{-1}, respectively (with 95% confidence intervals of ± 0.032 and $\pm 0.043\ \text{year}^{-1}$; Figure 11, and see the time series in Figure 9d). The long-term decrease in depressions in the Sikka archive is opposed by a long-term increase in lows, resulting in no trend in total LPS. Any trend in JRA-55 is substantially smaller than in the Sikka or IMD data sets and is not significant at the 95% confidence level (Figure 11); the trend in counts of

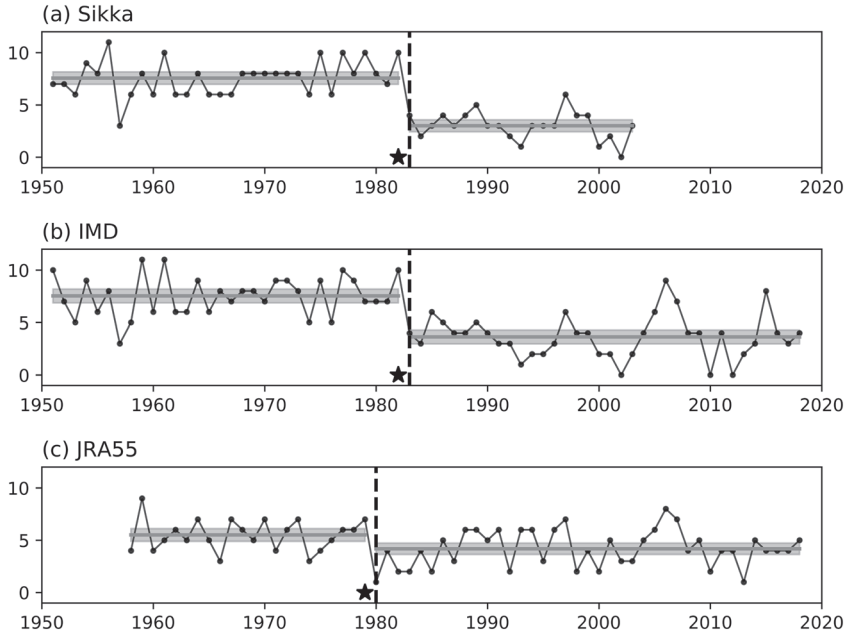

Figure 12. Illustration of a shift in depression counts around 1980. Year-to-year variation of depression counts (black line) in (a) the Sikka archive, (b) the IMD dataset, and (c) JRA-55. The vertical dashed line is the year of the mean shift in depression counts using binary change point detection. The star symbol marks the introduction of geostationary satellite data in the respective data set. The horizontal gray lines shows the summer mean value of depression counts in the given epoch, and shading shows the 95% confidence interval of the mean values.

depressions in JRA-55 is -0.021 year^{-1} with a 95% confidence interval of $\pm$0.024 year^{-1}). No statistically significant trend is seen in the total number of LPS forming each summer in JRA-55.

Although the Indian summer monsoon season is commonly defined as occurring June–September, with the Sikka archive available for only those months, it is possible that the results of our trend analysis would change if we used an extended season of May–October. Indeed, Xavier et al. (2007) argued that the primary effect of ENSO on Indian rainfall occurs via its influence on the duration of the rainy season, with La Niña events allowing it to extend into May and October. Including May and October in our trend analysis for the period starting in 1958 yields an increase in the magnitude of the depression count trends found in JRA-55 and the IMD data set, with the JRA-55 trend becoming significant at the 95% confidence level (Figure 11). The total number of LPS forming in this extended summer season in JRA-55 also shows a decreasing trend that is significant at the 95% confidence level, but there is no discernible trend in lows in JRA-55. We also repeated the trend assessment, using the longer May–October season, for all reanalyses for the shorter period starting in 1979, with little change in the results: Only ERA-Interim LPS show an increasing trend significant at the 95% confidence level.

We also analyze storm count trends using multiple detection algorithms, in order to explore the influence of parametric and structural uncertainty in the algorithm on our trend assessment. Specifically, we examine LPS counts obtained using the top five stream function-based algorithms, the top three geopotential height-based algorithms, and the top three MSLP-based algorithms. No algorithms applied to any reanalysis show a significant trend starting in 1979 (Figure S5). However, two of the nine algorithms applied to JRA-55 show a statistically significant decrease in LPS from 1958, and one of the nine shows a significant decrease in depression counts in that period. All of these trends are of similar magnitude to the those found in JRA-55 with our primary algorithm (Figure 11).

5.3.2. Change Point Detection

Like any reanalysis, JRA-55 assimilated data from an observational network that evolved over time, and we wish to consider whether this might affect any detected trends. For example, satellite data first started to be assimilated by JRA-55 around 1980, and there is a large reduction in depression counts in JRA-55 in that year (Figure 9d). We calculate the year and magnitude of a single long-term shift in the summer mean depression

count using a binary change point detection method (Truong et al., 2020), and find that the mean depression count undergoes a systematic reduction in the early 1980s all data sets: 1983 in IMD and the Sikka archive and 1980 in JRA-55 (Figure 12). The shift in the mean values is larger in the IMD data set (decreasing from 7.5 ± 0.7 to 3.6 ± 0.7 year^{-1}) and the Sikka archive (decreasing from 7.6 ± 0.6 to 3.0 ± 0.6 year^{-1}) and smallest in JRA-55 (decreasing from 5.5 ± 0.6 to 4.2 ± 0.5 year^{-1}). The shifts in all three data sets are statistically significant at the 95% confidence level. The shift in JRA-55 in 1980 is contemporaneous with the introduction of geostationary satellites observations to that reanalysis system in 1979 (Ebita et al., 2011), the date marked by the star in Figure 12c. Similarly, the IMD started using Indian geostationary satellite data in 1982, which is contemporaneous with the 1983 shift in depression counts in both the Sikka archive and the IMD data set (recall that the Sikka archive was constructed by analyzing MSLP maps obtained from the IMD). This suggests that the shift, and by association the linear trends discussed above, might be an artifact of changes in observational data sources. Formal attribution of these early-1980s shifts is beyond the scope of this manuscript, but these results suggest that further study is warranted.

6. Summary and Conclusions

Synoptic-scale monsoon LPS produce abundant rainfall over South Asia, making the identification of LPS in estimates of past and future atmospheric states an important task. Yet previous methods for tracking LPS have relied on subjective or automated methods not systematically assessed for skill or optimality (Hunt et al., 2016; Hurley & Boos, 2015; Mooley & Shukla, 1987; Praveen et al., 2015; Sikka, 2006). For example, multiple previous LPS data sets were based entirely on MSLP, even though LPS are known to have peak intensities several kilometers above the surface (Godbole, 1977). These issues become especially salient when examining multidecadal trends in LPS activity, because unintentional changes in a subjective method or trends in the observing network on which an underlying data set is based could bias an analyzed trend.

This study builds on previous literature by introducing a fast and objective tracking algorithm able to identify monsoon LPS in high-resolution data sets. The method is based on the feature tracking capabilities of the TempestExtremes package. A sensitivity analysis was performed to choose an optimal algorithm using multiple reanalyses of various spatial and temporal resolutions. A total of 512 algorithms (defined by different search variables and values for the closed contour criteria) are applied to four reanalyses for the training period of 1990–2003. Based on a skill score, the CSI, that compares the reanalyses with each other and with the Sikka archive (our reference data set), the optimal algorithm was found to use the 850 hPa stream function of horizontal wind. The LPS identified with this algorithm in reanalyses are found to match about 80% of LPS in the Sikka archive. The reanalyses track data sets also contain LPS not present in the Sikka archive. For instance, the ERA5 data set includes 57 lows and 10 depressions that are entirely missing in the Sikka archive. Composites of these LPS and the LPS present in the Sikka archive show similar dynamical structures, so we conclude that the algorithm correctly captures LPS in the atmospheric states represented by the reanalyses.

Characteristics of the LPS, including distributions of genesis frequency, track density, intensity, lifetime, and track length, are consistent across all reanalyses and are similar to results from the Sikka archive. The new reanalysis track data sets also reproduce previously reported monthly and basin-wise climatological variations of LPS characteristics. On interannual time scales, LPS counts in the reanalyses have weak correlation with the Sikka archive. This result may be due, in part, to LPS that are missing from the Sikka archive but that exist in most of the reanalyses. Indeed, we estimate that if only 20–30% of the storms in one data set are replaced with randomly distributed false alarms, this is expected to reduce the interannual correlation coefficient to 0.5 or lower. The better correspondence between the track data sets based on five different reanalyses, with horizontal resolutions ranging from 0.25° to 1.25°, gives confidence that the algorithm can consistently capture LPS in data sets with different resolutions.

Our examination of interannual variations in LPS genesis frequency, track length, and lifetimes illustrate the importance of assessing signals in multiple data sets. For the period starting in 1979, we find significantly higher LPS counts in pluvial years compared to drought years in four out of five reanalyses, in agreement with the longer period (1901–2003) analysis of Krishnamurthy and Ajayamohan (2010). We also find significantly higher LPS counts in La Niña years relative to El Niño years, again in four of five reanalyses and consistent with Krishnamurthy and Ajayamohan (2010). Associations between LPS counts and the Indian

Ocean Dipole are detected in only one reanalysis, despite the fact that Krishnan et al. (2011) and Hunt et al. (2016) reported enhanced depression activity in positive IOD years. The higher depression activity in El Niño years reported by Hunt et al. (2016) was also not seen in any of the reanalyses we examined.

Past studies of long-term trends in the IMD and Sikka data sets have found increases in the number of lows and decreases in the number of depressions (Prajeesh et al., 2013; Rajendra Kumar & Dash, 2001; Vishnu et al., 2016). Here, however, we do not detect statistically significant trends in summer counts of lows or depressions in any reanalysis for the period from 1979 onward (the Sikka archive has a strong decrease in depression counts and an increase in lows for that period). The JRA-55 reanalysis, which provides data starting in 1958, shows a statistically significant reduction in depression counts only when using an extended summer season (May–October), and this trend is about one quarter the magnitude of the trend seen in the IMD data set and Sikka archive. Furthermore, a binary change point detection analysis shows that the long-term decrease is consistent with a step-wise reduction in depression counts in the year following the introduction of geostationary satellite data into the data sets underlying the IMD, Sikka, and JRA-55 products. This suggests the possibility that no long-term reduction in depressions has occurred, and trends seen in existing data products may be artifacts of change in the observing network; further analysis is warranted.

The new and objective LPS data sets developed here have been made publicly available, together with the tracking algorithm, to allow their broad use in characterizing LPS activity and understanding LPS dynamics (doi:10.5281/zenodo.3890646). These data sets and the tracking algorithm may also be useful in assessing LPS activity in ensembles of global climate models and in characterizing and correcting bias in forecasts made by numerical weather prediction models. The future release of new reanalysis data for years preceding 1979, such as is expected for ERA5 (Hersbach & Dee, 2016), will also provide new opportunities to reexamine long-term trends in LPS activity, especially since those reanalyses include representations of historical climate forcings by greenhouse gas, aerosol, and land use changes.

Appendix A: Boundary Conditions for Stream Function Inversion

A practical challenge exists when computing the stream function, ψ, of the horizontal wind, $\vec{u}$, on a level of a vertical coordinate system that intersects the ground; boundary conditions must be imposed on that intersection when inverting the winds (or vorticity) to obtain ψ. That is, the uniqueness of the Helmholtz decomposition that holds in a spherical domain without boundaries breaks down, and a class of harmonic functions can be added to ψ while still allowing $\nabla^2\psi$ to correctly represent the local vertical vorticity. Numerous ways of dealing with this nonuniqueness have been proposed in the context of atmospheric and oceanic flow (Lynch, 1988). One method requires the velocity potential, ϕ, to vanish on the boundaries, minimizing the kinetic energy in the divergent part of the flow (Pedersen, 1971; Sangster, 1960). Another method requires ψ to be constant along a boundary (Watterson, 2001); this is appropriate when there is zero horizontal divergence along the boundary but is invalid in many cases having large vertical motion along physical boundaries, such as upwelling in coastal ocean regions (Li et al., 2006) or strong orographic ascent in the atmosphere. Lynch (1989) proposed a three-component partitioning into nondivergent, irrotational, and harmonic flow, while Li et al. (2006) made the two-component decomposition unique by introducing a constraint to the inversion problem that implicitly determines the boundary condition by minimizing the joint amplitude of ψ and ϕ.

Here we are concerned with domain boundaries created by the intersection of a pressure surface with topography, with the pressure surface lying at a sufficiently high altitude that the boundaries surround relatively small holes in the otherwise global, spherical domain. Unlike the regional atmospheric model problem in which ψ and ϕ are obtained in a subdomain of global, nonzero atmospheric flow, we know that no wind exists outside of our domain (i.e., beneath Earth's surface). We thus follow the suggestion of Morse and Feshbach (1953) and set the total wind outside the domain boundaries to 0 and invert $\vec{u}$ to obtain unique distributions of ψ and ϕ in the unbounded global domain. Some reanalyses (e.g., ERA-Interim) extrapolate winds beneath Earth's surface, so our choice involves replacing those extrapolated values with $\vec{u} = 0$. This choice results in nonzero values of the nondivergent and irrotational wind beneath Earth's surface; these two components sum to 0 in that region. This contrasts with methods that assumed nondivergent flow along the boundaries (Watterson, 2001), because we recognize that winds can horizontally converge along the topographic boundary at the grid scale of the data; such convergence is common along the Himalaya and Arakan mountains in

the summer monsoon. An important point is that our choice of $\vec{u}$ beneath Earth's surface, or equivalently of the boundary condition for ψ, has only minor effects on our numerical identification of vortices because that choice alters ψ only by addition of a function with zero curvature, and our identification algorithm involves finding local minima (i.e., regions of positive curvature) in the discretized stream function.

Appendix B: LPS Detection Program

The command-line syntax to obtain LPS tracks from a 6-hourly data set using TempestExtremes with a bash shell is as follows:

```
# Set a series of shell variables:
# File containing Streamfunction at 850 (PSI)
psifile="./psi.nc"

# File containing mean sea level pressure (msl)
pslfile="./msl.nc"

# File containing relative humidity at 850 hPa (RH)
rhfile="./RH850.nc"

# File containing surface wind field (u10, v10)
uvfile="./uvsurf.nc"

# File containing surface geopotential (zs)
zsfile="./geopotential_surface.nc"

# File containing land-sea fraction (lsm)
lsmfile="./land_sea.nc"

# Candidate file
candidatefile="./LPS_candidates.txt"

# Output file
outfile="./LPS_output.txt"

# Track file
trackfile="./LPS_track.txt"


# Detect LPS:
#   1) Search for candidates as minima in the streamfunction field
#   2) Merge candidates within 5 degrees
#   3) Output streamfunction minima at the candidate point,
#      sea level pressure minima within 3 degrees of the candidate point,
#      wind speed maxima within 3 degrees of candidate,
#      relative humidity averaged over the area within 3 degrees of candidate,
#      surface geopotential maximum within 2 degrees of candidate,
#      land-sea ratio at candidate point, and
#.     minimum sea level pressure location.
```

```
$path-to-TEMPEST-bin/DetectNodes
    --in_data "$psifile;$pslfile;$rhfile;$uvfile;$zsfile;$lsmfile"
    --out $candidatefile
    --searchbymin "PSI" --mergedist 5.0
    --closedcontourcmd "PSI,12.5e5,10,0"
    --outputcmd "PSI,min,0;msl,min,3;RH,avg,3;zs,max,2;lsm,max,0;
     _VECMAG(u10,v10),max,3;msl,minix,3.0"
#Stitch candidates to make tracks:
#   1) With a maximum distance of 3.0 degrees between in-sequence candidates
#   2) With a minimum length of 5 time points
#       (ensures track lasts longer than 1 day in six-hourly data)
#   3) With a maximum gap size of 2 time points (12 hours)
#   4) With the surface geopotential maximum less than 8000 m^2 s^{-2}
#       for at least 4 time steps along the track
#   5) With the relative humidity higher than 85% for at least 4 time steps
#       along the track.

$path-to-TEMPEST-bin/StitchNodes --in $candidatefile --out $outfile
    --format "i,j,lon,lat,strf850,slp,rh,zs,lsm,sp,minmslix"
    --range 3.0 --minlength 5 --maxgap 2
    --threshold "zs,<=,8000.,4;rh,>=,85,4"


# Calculate some derived quantities using track data:
# count the closed contours of MSLP, calculate ACEPSL, ACE, PDI, IKE
# ACEPSL = 1e-4 * (1.94384 kt/(m/s) * (3.92 * (1016 - PSL)^0.644))^2
  if PSL < 1016. Here PSL is the minimum surface pressure at the point
  of detection in hPa. This formula leverages the TC wind-pressure
  relationship to provide a proxy for ACE.
# ACE = 1e-4 * (1.94384 kt/(m/s) * Umax)^2, where Umax is the maximum
  instantaneous wind speed magnitude within the three degree radius (in m/s).
# PDI = Umax^3, where Umax is the maximum instantaneous windspeed magnitude
  within the three degree radius (in m/s)
# IKE = sum_i 0.5 * U_i^2 * area_i, where the sum is taken over all grid boxes
  within the given radius, U_i is the wind magnitude in that grid cell,
  and area_i is the area of the grid cell (in m^2).

$path-to-TEMPEST-bin/NodeFileEditor --in_file $outfile --out_file $trackfile
    --in_data "$pslfile;$uvfile"
    --in_fmt "lon,lat,strf850,slp,rh,zs,lsm,sp,minmslix"
    --calculate "deltaslp=max_closed_contour_delta(msl,10,minmslix);
        acepsl=eval_acepsl(msl,10.0);
        ace=eval_ace(u10,v10,3.0);
        pdi=eval_pdi(u10,v10,3.0);
        ike=eval_ike(u10,v10,3.0)"
    --out_fmt "lon,lat,strf850,slp,deltaslp,sp,rh,zs,lsm,acepsl,ace,pdi,ike"
```

Data Availability Statement

The India Meteorological Department record of monsoon depression tracks was downloaded from the IMD website (at https://www.imd.gov.in). The Sikka archive was obtained from Sikka (2006). The ERA-Interim data set was downloaded from the ECMWF website (at https://apps.ecmwf.int/datasets/data/ interim-full-daily). The MERRA-2 data set was downloaded from NASA's Goddard Earth Sciences Data and Information Services Center (GES DISC) website (at https://disc.gsfc.nasa.gov/datasets? keywords=%

22MERRA-2%22page=1source=Models%2FAnalyses%20MERRA-2). The ERA5 data set was obtained from the Copernicus Climate Change Service Climate Data Store (CDS) website (at https://cds.climate.copernicus.eu/cdsapp#!/home), accessed on 1 March 2019. The CFSR and JRA-55 reanalysis were obtained from the Research Data Archive that is maintained by the Computational and Information Systems Laboratory at the National Center for Atmospheric Research (NCAR). The data are available online (at https://rda.ucar.edu). The HadISST data set was downloaded from the website of NCAR (at https://climatedataguide.ucar.edu/climate-data/sst-data-hadisst-v11). The track data sets created in this work are available through the Zenodo repository (doi:10.5281/zenodo.3890646).

Acknowledgments

The authors gratefully acknowledge the financial support given by the Earth System Science Organization, Ministry of Earth Sciences, Government of India (Grant IITM/MM-II/Univ_California_USA/INT-3) to conduct this research under Monsoon Mission. This material is based upon work supported by the U.S. Department of Energy, Office of Science, Office of Biological and Environmental Research, Climate and Environmental Sciences Division, Regional and Global Model Analysis Program, under Award DE-SC0019367. It used resources of the National Energy Research Scientific Computing Center (NERSC), which is a DOE Office of Science User Facility.

References

Bengtsson, L., Böttger, H., & Kanamitsu, M. (1982). Simulation of hurricane-type vortices in a general circulation model. *Tellus*, *34*(5), 440–457.

Berry, G. J., Reeder, M. J., & Jakob, C. (2012). Coherent synoptic disturbances in the Australian monsoon. *Journal of Climate*, *25*(24), 8409–8421.

Bollasina, M., & Nigam, S. (2009). Indian Ocean SST, evaporation, and precipitation during the South Asian summer monsoon in IPCC-AR4 coupled simulations. *Climate Dynamics*, *33*(7-8), 1017.

Boos, W. R., Hurley, J. V., & Murthy, V. S. (2015). Adiabatic westward drift of Indian monsoon depressions. *Quarterly Journal of the Royal Meteorological Society*, *141*(689), 1035–1048.

Broccoli, A. J., & Manabe, S. (1990). Can existing climate models be used to study anthropogenic changes in tropical cyclone climate?. *Geophysical Research Letters*, *17*(11), 1917–1920.

Chavas, D. R., Reed, K. A., & Knaff, J. A. (2017). Physical understanding of the tropical cyclone wind-pressure relationship. *Nature Communications*, *8*(1), 1–11.

Cohen, N. Y., & Boos, W. R. (2014). Has the number of Indian summer monsoon depressions decreased over the last 30 years? *Geophysical Research Letters*, *41*, 7846–7853. https://doi.org/10.1002/2014GL061895

Dee, D. P., Uppala, S. M., Simmons, A. J., Berrisford, P., Poli, P., Kobayashi, S., et al. (2011). The ERA-Interim reanalysis: Configuration and performance of the data assimilation system. *Quarterly Journal of the Royal Meteorological Society*, *137*(656), 553–597.

Delgado, S., Landsea, C. W., & Willoughby, H. (2018). Reanalysis of the 1954–63 Atlantic hurricane seasons. *Journal of Climate*, *31*(11), 4177–4192.

Di Luca, A., Evans, J. P., Pepler, A., Alexander, L., & Argüeso, D. (2015). Resolution sensitivity of cyclone climatology over eastern Australia using six reanalysis products. *Journal of Climate*, *28*(24), 9530–9549.

Ebita, A., Kobayashi, S., Ota, Y., Moriya, M., Kumabe, R., Onogi, K., et al. (2011). The Japanese 55-year reanalysis JRA-55: An interim report. *Sola*, *7*, 149–152.

Gelaro, R., McCarty, W., Suárez, M. J., Todling, R., Molod, A., Takacs, L., et al. (2017). The Modern-Era Retrospective Analysis for Research and Applications, Version 2 (MERRA-2). *Journal of Climate*, *30*(14), 5419–5454.

Godbole, R. V. (1977). The composite structure of the monsoon depression. *Tellus*, *29*(1), 25–40.

Hagen, A. B., Strahan-Sakoskie, D., & Luckett, C. (2012). A reanalysis of the 1944–53 Atlantic hurricane seasons—The first decade of aircraft reconnaissance. *Journal of Climate*, *25*(13), 4441–4460.

Hersbach, H., Bell, W., Berrisford, P., Horányi, A., Sabater, J. M., Nicolas, J., et al. (2019). Global reanalysis: Goodbye ERA-Interim, hello ERA5. *ECMWF Newsletter*, *159*, 17–24. https://doi.org/10.21957/vf291hehd7

Hersbach, H., & Dee, D. (2016). ERA5 reanalysis is in production. *ECMWF Newsletter*, *147*, 5–6. Reading, UK.

Hodges, K. I. (1995). Feature tracking on the unit sphere. *Monthly Weather Review*, *123*(12), 3458–3465.

Hodges, K. I. (1998). Feature-point detection using distance transforms: Application to tracking tropical convective complexes. *Monthly Weather Review*, *126*(3), 785–795.

Houze Jr, R. A., Rasmussen, K. L., Medina, S., Brodzik, S. R., & Romatschke, U. (2011). Anomalous atmospheric events leading to the summer 2010 floods in Pakistan. *Bulletin of the American Meteorological Society*, *92*(3), 291–298.

Hunt, M., Turner, A. G., Inness, P. M., Parker, D. E., & Levine, R. C. (2016). On the structure and dynamics of Indian monsoon depressions. *Monthly Weather Review*, *144*(9), 3391–3416.

Hurley, J. V., & Boos, W. R. (2015). A global climatology of monsoon low-pressure systems. *Quarterly Journal of the Royal Meteorological Society*, *141*(689), 1049–1064.

India Meteorological Department (2011). Tracks of cyclones and depressions over north Indian Ocean (from 1891 onwards), Tech. Note Version 2.0. Cyclone Warning and Research Centre India Meteorological Department Regional Meteorological Centre, Chennai, India.

Jadhav, S. K., & Munot, A. A. (2009). Warming SST of Bay of Bengal and decrease in formation of cyclonic disturbances over the Indian region during southwest monsoon season. *Theoretical and Applied Climatology*, *96*(3-4), 327–336.

Kobayashi, S., Ota, Y., Harada, Y., Ebita, A., Moriya, M., Onoda, H., et al. (2015). The JRA-55 reanalysis: General specifications and basic characteristics. *Journal of the Meteorological Society of Japan Series II*, *93*(1), 5–48.

Krishnamurthy, V., & Ajayamohan, R. S. (2010). Composite structure of monsoon low pressure systems and its relation to Indian rainfall. *Journal of Climate*, *23*(16), 4285–4305.

Krishnan, R., Ayantika, D. C., Kumar, V., & Pokhrel, S. (2011). The long-lived monsoon depressions of 2006 and their linkage with the Indian Ocean Dipole. *International Journal of Climatology*, *31*(9), 1334–1352.

Landsea, C. W., Glenn, D. A., Bredemeyer, W., Chenoweth, M., Ellis, R., Gamache, J., et al. (2008). A reanalysis of the 1911–20 Atlantic hurricane database. *Journal of Climate*, *21*(10), 2138–2168.

Landsea, C. W., Hagen, A., Bredemeyer, W., Carrasco, C., Glenn, D. A., Santiago, A., et al. (2014). A reanalysis of the 1931–43 Atlantic hurricane database. *Journal of Climate*, *27*(16), 6093–6118.

Li, H., Chen, W., & Shen, I.-F. (2006). Segmentation of discrete vector fields. *IEEE Transactions on Visualization and Computer Graphics*, *12*(3), 289–300.

Lynch, P. (1988). Deducing the wind from vorticity and divergence. *Monthly Weather Review*, *116*(1), 86–93.

Lynch, P. (1989). Partitioning the wind in a limited domain. *Monthly Weather Review*, *117*(7), 1492–1500.

Manganello, J. V., Cash, B. A., Hodges, K. I., & Kinter, J. L. (2019). Seasonal forecasts of North Atlantic tropical cyclone activity in the North American multi-model ensemble. *Climate Dynamics*, *53*(12), 7169–7184.
McCarty, W., Coy, L., Gelaro, R., Huang, A., Merkova, D., Smith, E. B., et al. (2016). MERRA-2 input observations: Summary and assessment (*NASA/TM-2016-104606*): NASA Tech. Rep. Series on Global Modeling and Data Assimilation.
Michaelis, A. C., & Lackmann, G. M. (2019). Climatological changes in the extratropical transition of tropical cyclones in high-resolution global simulations. *Journal of Climate*, *32*(24), 8733–8753.
Mooley, D. A. (1973). Some aspects of Indian monsoon depression and associated rainfall. *Monthly Weather Review*, *101*, 271–280.
Mooley, D. A., & Shukla, J. (1987). Characteristics of the westward-moving summer monsoon low pressure systems over the Indian region and their relationship with the monsoon rainfall. University of Maryland, Center for Ocean-Land.-Atmosphere Interactions Tech. Rep., 128 pp.
Morse, P. M., & Feshbach, H. (1953). Methods of theoretical physics [Vol 1–2]. McGraw-Hill, New York.
Pedersen, K. (1971). Balanced systems of equations for the atmospheric motion—A numerical experiment, and an analytical discussion (linearized two level model for atmospheric motion equations systems, using Psi-balanced system for 24 hour forecast). *Geofysiske Publikasjoner(Geophysica Norvegica)*, *28*, 1–12.
Prajeesh, A. G., Ashok, K., & Rao, D. V. B. (2013). Falling monsoon depression frequency: A Gray-Sikka conditions perspective. *Scientific Reports*, *3*, 2989.
Praveen, V., Sandeep, S., & Ajayamohan, R. S. (2015). On the relationship between mean monsoon precipitation and low pressure systems in climate model simulations. *Journal of Climate*, *28*(13), 5305–5324.
Rácz, Z., & Smith, R. K. (1999). The dynamics of heat lows. *Quarterly Journal of the Royal Meteorological Society*, *125*(553), 225–252.
Rajendra Kumar, J., & Dash, S. K. (2001). Interdecadal variations of characteristics of monsoon disturbances and their epochal relationships with rainfall and other tropical features. *International Journal of Climatology*, *21*(6), 759–771.
Ramage, C. S. (1971). *Monsoon meteorology (international geophysics series; v. 15)*. New York, USA: Academic Press.
Ramanathan, V., Chung, C., Kim, D., Bettge, T., Buja, L., Kiehl, J. T., et al. (2005). Atmospheric brown clouds: Impacts on South Asian climate and hydrological cycle. *Proceedings of the National Academy of Sciences*, *102*(15), 5326–5333.
Rastogi, D., Ashfaq, M., Leung, L. R., Ghosh, S., Saha, A., Hodges, K., & Evans, K. (2018). Characteristics of Bay of Bengal monsoon depressions in the 21st century. *Geophysical Research Letters*, *45*, 6637–6645. https://doi.org/10.1029/2018GL078756
Rayner, N. A., Parker, D. E., Horton, E. B., Folland, C. K., Alexander, L. V., Rowell, D. P., et al. (2003). Global analyses of sea surface temperature, sea ice, and night marine air temperature since the late nineteenth century. *Journal of Geophysical Research*, *108*(D14), 4407. https://doi.org/10.1029/2002JD002670
Saha, S., Moorthi, S., Pan, H.-L., Wu, X., Wang, J., Nadiga, S., et al. (2010). The NCEP climate forecast system reanalysis. *Bulletin of the American Meteorological Society*, *91*(8), 1015–1058.
Saji, N. H., Goswami, B. N., Vinayachandran, P. N., & Yamagata, T. (1999). A dipole mode in the tropical Indian Ocean. *Nature*, *401*(6751), 360.
Sandeep, S., Ajayamohan, R. S., Boos, W. R., Sabin, T. P., & Praveen, V. (2018). Decline and poleward shift in Indian summer monsoon synoptic activity in a warming climate. *Proceedings of the National Academy of Sciences*, *115*(11), 2681–2686.
Sanders, F. (1984). Quasi-geostrophic diagnosis of the monsoon depression of 5–8 July 1979. *Journal of the Atmospheric Sciences*, *41*(4), 538–552.
Sangster, W. E. (1960). A method of representing the horizontal pressure force without reduction of station pressures to sea level. *Journal of Meteorology*, *17*(2), 166–176.
Sikka, D. R. (1978). Some aspects of the life history, structure and movement of monsoon depressions. *Monsoon dynamics* (pp. 1501–1529). Basel: Springer.
Sikka, D. R. (2006). A study on the monsoon low pressure systems over the Indian region and their relationship with drought and excess monsoon seasonal rainfall. Center for Ocean-Land-Atmosphere Studies, Tech. Rep. 217, 145 pp.
Thorncroft, C., & Hodges, K. (2001). African easterly wave variability and its relationship to Atlantic tropical cyclone activity. *Journal of Climate*, *14*(6), 1166–1179.
Truong, C., Oudre, L., & Vayatis, N. (2020). Selective review of offline change point detection methods. *Signal Processing*, *167*, 107299. https://doi.org/10.1016/j.sigpro.2019.107299
Ullrich, P. A., & Zarzycki, C. M. (2017). TempestExtremes: A framework for scale-insensitive pointwise feature tracking on unstructured grids. *Geoscientific Model Development*, *10*(3), 1069.
Vishnu, S., Francis, P. A., Shenoi, S. S. C., & Ramakrishna, S. S. V. S. (2016). On the decreasing trend of the number of monsoon depressions in the Bay of Bengal. *Environmental Research Letters*, *11*(1), 014011.
Vishnu, S., Francis, P. A., Shenoi, S. C., & Ramakrishna, S. S. V. S. (2018). On the relationship between the Pacific Decadal Oscillation and monsoon depressions over the Bay of Bengal. *Atmospheric Science Letters*, *19*(7), e825.
Watterson, I. G. (2001). Decomposition of global ocean currents using a simple iterative method. *Journal of Atmospheric and Oceanic Technology*, *18*(4), 691–703.
Webster, P. J., Moore, A. M., Loschnigg, J. P., & Leben, R. R. (1999). Coupled ocean–atmosphere dynamics in the Indian Ocean during 1997–98. *Nature*, *401*(6751), 356.
Xavier, P. K., Marzin, C., & Goswami, B. N. (2007). An objective definition of the Indian summer monsoon season and a new perspective on the ENSO–monsoon relationship. *Quarterly Journal of the Royal Meteorological Society*, *133*(624), 749–764.
Yoon, J.-H., & Chen, T.-C. (2005). Water vapor budget of the Indian monsoon depression. *Tellus A*, *57*(5), 770–782.
Zarzycki, C. M., Thatcher, D. R., & Jablonowski, C. (2017). Objective tropical cyclone extratropical transition detection in high-resolution reanalysis and climate model data. *Journal of Advances in Modeling Earth Systems*, *9*, 130–148. https://doi.org/10.1002/2016MS000775
Zarzycki, C. M., & Ullrich, P. A. (2017). Assessing sensitivities in algorithmic detection of tropical cyclones in climate data. *Geophysical Research Letters*, *44*, 1141–1149. https://doi.org/10.1002/2016GL071606